Gas and Particle Flow in a Spray Roaster

S. Johansson[1†], L. G. Westerberg[1], and T. S. Lundström[1]

Division of Fluid and Experimental Mechanics, Luleå University of Technology, SE-971 87 Luleå, Sweden

† *Corresponding Author Email*: *Simon.Johansson@ltu.se*

ABSTRACT

In the steel industry, waste hydrochloric acid is produced through the process to pickle steel slabs for removal of corrosion. Regenerated hydrochloric acid is obtained by separating the chloride gas from the waste product through spray roasting. This process also produces a by-product in the form of iron oxide which is sold to different industries. The present study is a continuation of a study arising from the need to better understand the dynamics inside the regeneration reactor, which in turn will improve possibilities to optimize the regeneration process, which to date has been manually adjusted by trial and error. In this study the velocity and temperature distribution inside the reactor is numerically modelled together with the droplet motion through the reactor. The main objective is to investigate the influence of a changed spray nozzle position on the flow characteristics of the continuous and dispersed phase, and the relation between temperature and energy efficiency and the regeneration process. Numerical models of the type of flow present in the regeneration reactor are not represented to any major extent in the literature, making the present study relevant to the engineers and researchers active in the steel industry and the application in question.

Keywords: Two-phase flow, Hydrochloric acid regeneration, Particle transport, Energy efficiency, Spray nozzle position.

NOMENCLATURE

A_f	cross section area of a particle
$C_{\varepsilon1}, C_{\varepsilon2}$	model constants
CFD	computational Fluid Dynamics
e	error
f_i	external force
GCI	grid Convergence Index
h	latent heat of water
h_c	heat transfer due to convection
h_r	heat transfer due to radiation
k	turbulent kinetic energy
k_f	thermal conductivity
L	characteristic length
M	million
Nu	Nusselt number
p	order of solution
P	ensamble-averaged pressure
Pr	Prandtl number
r	radial co-ordinate
r_{ij}	ratio between indexed mesh sizes
Re	Reynolds number
Re_p	particle Raynolds number

RNG	Renormalized Group
RSM	Reynolds Stress Model
RANS	Reynolds Averaged Navier- Stokes
S	rate of strain
T	temperature
T_a	volume averaged temperature
U_i	ensamble-averaged velocity
u_i	velocity fluctuations
$\overline{u_i u_j}$	turbulent Reynolds stresses
$v_{p,f}$	Particle/fluid velocity
v_p^0	particle velocity at the beginning of the cell
ε	dissipation rate of turbulent energy
ε_m	surface emissivity
λ	thermal conductivity of the fluid
μ	laminar dynamic viscosity
μ_t	turbulent viscosity
ρ	fluid density
$\sigma_\varepsilon, \sigma_k$	model constants
σ_b	Stefan-Bolzmann constant
τ	aerodynamic relaxation time
$\%_m$	mass percentage

1. INTRODUCTION

Hydrochloric acid (HCl) is used in the steel industry to remove iron oxide complexes from sheets aimed for high strength steels Johansson (2010). The process is called *pickling* and implies that steel sheets are pulled through a container with acid whereupon the iron oxide on the metal surface reacts with the acid and dissolves into it. In steel industries it is generally preferred that the waste HCl is regenerated rather than being shipped away for destruction, as the latter is a more expensive alternative. The regeneration process in question in the present study is carried out using the *spray roasting* technique, a process which is driven by four gas burners placed symmetrically along the periphery of the reactor at a level just above the conical section; see Fig. 1. Waste acid is sprayed into the reactor through spray nozzles near the top, while chloride gas is collected at the top of the reactor. The by-product in the form of hematite, i.e. the mineral form of iron (III) oxide (Fe_2O_3), is produced and collected at the bottom of the reactor. The hematite is sold and used in e.g. the electronics industry and as filling material in road constructions. The by-product from the regeneration process is thus recycled, contributing to environmental sustainability and to economic benefits from HCl regeneration.

Up to around the 1960s, sulphuric acid (H_2SO_4) was used in most pickling plants, but nowadays HCl is the most used acid Kladnig (2008). The physical details of the regeneration process are not known. The quality of the regeneration/ drying process which directly mirrors the quality of the iron oxide is of certain importance since the profitability of the product is dependent on it. The process is tuned by adjusting the inflow of waste acid (speed and direction) and the burner mass flow rate. To better understand the drying process, it is essential to have a picture of the gas flow dynamics inside the reactor. The flow behaviour inside the reactor is also of interest from a specifically fluid mechanical perspective, as it is characterized by a complex flow including a turbulent swirling motion. Only a few studies have been presented that scrutinize the regeneration process in the spray roaster. Nevertheless the regeneration process itself in terms of different approaches has attracted more attention within the research community in question. Two ways of regenerating HCl, through the membrane and pyrometallurgical techniques respectively, were presented in the work by Regel-Rosocka (2010). Other acid regeneration processes are theprecipitation/neutralization, and evaporation processes as described by Regel-Rosocka (2010) where it is shown that the pyrometallurgical techniques can be carried out in two ways, using fluidized beds and the spray roasting process respec-

tively two techniques which are described in detail by Kladnig (2008). In terms of numerical simulations of the regeneration process,Beck *et al.*(2007b) and Beck *et al.*(2007a) have used Computational Fluid Dynamics (CFD) to model the flow in the reactor with special emphasis on the coupling to the chemistry of the pickling process and the regeneration of the waste product. Recently Shiemann *et al.* (2012) performed a dual experimental and numerical study of spray roasting of $FeCl_2$, in which a laboratory scale model was used. Numerical models of the regeneration chemistry, in isolation or in combination with the reactor flow and the thermal dynamics, are relatively scarce in the literature. In addition to the work by Shiemann *et al.* (2012) cited above, Beck *et al.* (2007b) and Beck *et al.* (2007a) have in their studies focused closely on the process chemistry.

The present study is part of an overall approach of building a full numerical model of the regeneration process, and is a development of the work made by Johansson *et al.* (2010) and Westerberg *et al.* (2011), who designed a first numerical approach towards resolving the flow dynamics in the regeneration reactor together with the temperature and particle distribution. The focus in the present study is on the change in flow and temperature dynamics inside the reactor due to a changed spray nozzle location, and their impact on droplet motion through the reactor together with the impact on the energy efficiency. The numerical models in the present study are made with specifications from an existing plant. There are however many similar plants around the world that works on the same principles, but the dimensions might be different depending on the need of regeneration capacity of HCl.

CFD is generally a very useful tool to investigate both fundamental fluid flow properties and problems related to engineering applications. Modern codes are also highly suitable for multiphysical approaches like the present study. To exemplify the versatility of recent CFD simulations we highlight the following studies: by Gibson and Schild (2009) using CFD in astrophysical applications, Stouffs (2011) on hot air engines, Marjavaara *et al.* (2007) on hydraulic diffusers, Avinash *et al.* (2013) on Bingham flows, Choudhury and Hazarika (2013) on multi-physical magnetohydrodynamic flows, and Lundström *et al.* (2010) on fish guiding devices.

2. SET-UP

By resolving the temperature and velocity profiles inside the reactor in combination with particle transport, the effect of changing the nozzle positions at the top of the reactor on these quantities will be investigated. Variables in focus are the outlet temperature and droplet position and time taken
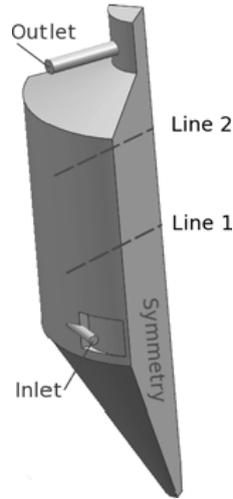
Fig. 1. Schematic view of the reactor geometry represented by one quarter of the domain. The spray roasting process is driven by the four burners placed along the periphery of the reactor. Waste acid is injected through spray nozzles at the top of the reactor. Chloride gas is collected at the outflow location while precipitated solid iron oxide falls to the bottom of the reactor, where it is collected.

for the droplets to fully evaporate. The outlet is set perpendicular to gravity in order to reduce the inflow of cold air into the process; see Fig. 1. The outlet temperature is of certain interest with respect to the regeneration process, since the thermal losses have to be minimized in order for the process to be as efficient as possible. Furthermore, for fuel efficiency, it is of particular interest to investigate the wall temperature and related heat loss through the wall. Droplet evaporation time and position are important, since the quality of the particles has to be uniform; which means that their trajectories have to be as similar as possible. It is also important that particles are evaporated before they hit the wall in order to reduce agglomeration, which can cause problems. With regard to the velocity, the vertical component is most significant, since it together with gravity transports the droplets through the process. The whole-field temperature distribution is also of importance since it gives information about where particles evaporate.

3. GOVERNING EQUATIONS AND NUMERICS

The simulations are carried out with the commercially available numerical code ANSYS CFX-13. The fluid is considered incompressible as the Mach number of the flow is significantly below 0.1, leading to negligible changes in fluid density due to compression. Considering an unsteady flow of an incompressible Newtonian fluid, the Reynolds-

average Navier-Stokes (RANS) equations are written as

$$\rho \frac{\partial U_i}{\partial t} + \rho \frac{\partial U_j U_i}{\partial x_j} = \rho f_i +$$
$$\frac{\partial}{\partial x_j} \left[-P\delta_{ij} + \mu \left(\frac{\partial U_i}{\partial x_j} + \frac{\partial U_j}{\partial x_i} \right) - \rho \overline{u_i u_j} \right] \quad (1)$$

where ρ is the density of the fluid, μ the laminar dynamic viscosity, P the ensemble-averaged pressure, U_i and f_i the ensemble-averaged velocity and external force components, and u_i the fluctuating velocity. The last term on the right hand side is turbulent (*Reynolds*) stresses due to the fluctuations in velocity field, which are determined according to the Boussinesq eddy viscosity assumption. The continuity and energy equations additionally apply to the RANS equations.

3.1 Turbulence Model

The two-equation model $k - \varepsilon$ is one of the most used turbulence models today as it is applicable to a large variety of flow scenarios, and is also cheap to use in terms of computational cost. Today the $k - \varepsilon$ model is the more common name for a family of special variations of the model as originally described. The $k - \varepsilon$ model has been tailored to work for different flow scenarios. One example is the Renormalized Group (RNG) $k - \varepsilon$ turbulence model which is sensitive enough to account for turbulent flow on a smaller scale through the re-normalized Navier-Stokes equations. The $k - \varepsilon$ model is written as

$$\frac{\partial(\rho k)}{\partial t} + \frac{\partial(\rho U_j k)}{\partial x_j} = \frac{\partial}{\partial x_j} \left[\left(\mu + \frac{\mu_t}{\sigma_k} \right) \frac{\partial k}{\partial x_j} \right] + P_k - \rho \varepsilon$$
$$(2)$$

$$\frac{\partial(\rho \varepsilon)}{\partial t} + \frac{\partial(\rho U_j \varepsilon)}{\partial x_j} = \frac{\partial}{\partial x_j} \left[\left(\mu + \frac{\mu_t}{\sigma_\varepsilon} \right) \frac{\partial \varepsilon}{\partial x_j} \right] +$$
$$+ \frac{k}{\varepsilon} (C_{\varepsilon 1} P_k - C_{\varepsilon 2} \rho \varepsilon) \quad (3)$$

where μ_t is the turbulent viscosity and σ_ε, σ_k, $\sigma_{\varepsilon 1}$ and $\sigma_{\varepsilon 2}$ are model constants Launder and Spalding (1974). Two variants of the $k - \varepsilon$ model are represented by the Renormalized Group (RNG) model introduced above, and the Realizable model respectively Yakhot *et al.* (1992), Shih *et al.* (1995). These models introduce the rate of strain $S = (S_{ij} S_{ij})^{1/2}$ into one of the constants. The Realizable $k - \varepsilon$ model introduces S to $\sigma_{\varepsilon 1}$ through a set of equations while the RNG $k - \varepsilon$ model introduces S into the constant $\sigma_{\varepsilon 2}$. For the application of swirling drying flow, Huang *et al.* (2004) presented

a comparison of how these three $k - \varepsilon$ turbulence models perform as compared to a more advanced Reynolds Stress Model (RSM). Experimental results showed that the RNG $k - \varepsilon$ turbulence model performs better than the standard $k - \varepsilon$ model and the Realizable $k - \varepsilon$ model, and almost as good as the more computationally costly RSM. It was also shown that the standard $k - \varepsilon$ model and the Realizable $k - \varepsilon$ model under-predicted the velocity in the inner region of the swirling velocity field. In this paper, the RNG $k - \varepsilon$ model is considered with respect to the actual application of swirling (spray) drying flow.

The Reynolds number for the continuous phase is of the order of 10^5 at the inlet level (top of the reactor), while the corresponding value at the burner level is of the order of $5 \cdot 10^5$.

3.2 Coupling Between Phases

The continuous phase is treated as Eulerian while the dispersed phase is modelled with a Lagrangian approach where the dispersed phase is solved every fifth iteration of the continuous phase. The phases are two-way coupled so that the dispersed phase is not only affected by the continuous phase but also contributes to the continuous phase by adding or subtracting source terms into the momentum, continuity and energy equations Sommerfeld *et al.* (2008). A turbulence model solely for the dispersed phase is not considered. The particles velocity is calculated through the analytical solution of the particle momentum equation

$$v_p = v_f + \left(v_p^0 - v_f\right)e^{\frac{\delta t}{\tau}} + F_{all}\left(1 - e^{\frac{\delta t}{\tau}}\right), \qquad (4)$$

where index p and f denotes particles and fluid respectively. 0 is the particle velocity at the beginning of the cell and τ the aerodynamic relaxation time. F_{all} is the sum of forces acting on the particles in this case buoyancy and drag which are calculated as

$$F_B = (m_p - m_f)g, \qquad (5)$$

$$F_D = \frac{1}{2}C_D \rho_f A_f \left|v_f - v_p\right|(v_f - v_p), \qquad (6)$$

where C_D is the drag coefficient and A_f the cross section area of the particle. The convective heat transfer is calculated by

$$Q_C = \pi d\lambda Nu(T_f - T_p), \qquad (7)$$

where λ is thermal conductivity of the fluid and Nu the Nusselt number which is calculated with

the Ranz-Marshall correlation according to Tosun (2002)

$$Nu = 2 + 0.6Re_p^{\frac{1}{2}}Pr^{\frac{1}{3}}. \qquad (8)$$

Here Re_p and Pr is the Reynolds number based on the particle diameter and the Prandtl number respectively. The type mass transfer from drop to continuous phase is determined by the Antoines equation

$$p_{vap} = p_{scale}e^{A\frac{B}{T_d - C}}, \qquad (9)$$

where A, B and C are constants; see Johansson 2010. If the exponential term is larger than 1 the vapor pressure p_{vap} is larger than the ambient pressure and boiling will occur, resulting in

$$\frac{dm_d}{dt} = -\frac{Q_C}{h}, \qquad (10)$$

where h is the latent heat of water. In the present paper boiling is the dominant mass transfer. For details about the non-boiling mass transfer readers are referred to Abrahamzon and Sirigano (1988). Mass, heat and the forces are introduced to the momentum-, continuity and energy equation as sources or sinks.

4. GEOMETRY, MESH AND BOUNDARY CONDITIONS

4.1 Geometry and Simulation Model

The reactor sketched in Fig. 1 has a total height of 18.5 m and a middle section 8.8 m in height, and has a radius of 4.3 m. The bottom section has a height of 6.8 m and a bottom radius of 0.23 m. The burners are placed 7.9 m from the bottom of the reactor. Each nozzle plate consists of four nozzles respectively, and is attached to the tip of a lance at the top of the reactor. There are four lances in total, which are placed symmetrically at a distance (in the radial direction) of 1.5 m from the center. In this study, two additional nozzle positions are simulated: $r = 0.5$ m and $r = 3.0$ m respectively. The simulation model described below is well investigated in terms of grid independency in and validated with the work by Huang *et al.* (2004), who used a lab-scale model of a spray dryer for experimental modelling. Validation with measurements in the reactor in question has not been carried with the exception of the temperature data presented in Johansson *et al.* (2010). Obtaining experimental results of the variables analysed in this study is not trivial due to the extremely hostile environment inside the reactor and requires a separate approach to be presented in a future publication. In this paper,

the quality and trust work is focused on the grid independency and validation with data from the lab-scale model that Huang *et al.* (2004) used. In Table 1, results from the grid study are presented. The results are from simulations with 10.6M, 6.4M and 1.3M nodes respectively. For the quality and trust in computational flow calculations it is highly important that the numerical model should show grid independency characteristics, meaning that the result for a chosen variable changes with the grid size up to a certain number of nodes. Grid independency is usually investigated using the Richardson extrapolation method. Results from the Richardson extrapolation study are presented in Table 1. In the present study the mesh with 6.4M nodes is used. For details of the Richardson extrapolation method we refer to Ferziger and Peric (2002) .

Table 1 Results from the Richardson extrapolation where r is the ratio between indexed mesh sizes, T_a the volume averaged temperature, p the order of the solution, e the error and GCI the Grid Convergence Index. Subscripts 4, 5 and 6 denote the mesh number and *ext* denotes extrapolated values. Mesh #4 corresponds to the 1.3M grid, mesh #5 the 6.4M grid, and mesh #6 the 10.6M grid respectively.

r_{12}	r_{32}	$T_{a_{mesh6}}$	$T_{a_{mesh5}}$	$T_{a_{mesh4}}$
1.16	1.75	797.05	800.79	830.97
$T_{a_{ext}}$	$T_{a_{present}}$	p	e_{56}	$e_{56_{ext}}$
791.94	791.46	2.92	0.47%	0.64%
$GCI_{56_{ext}}$	—	—	—	—
0.8%	—	—	—	—

4.2 Mesh

ANSYS ICEM CFD was used to create the meshes for the simulations. The geometry is complex at the inlet region, due to the inflow of burner gas and the location of a so called kick-out designed to redirect the flow in order to avoid inflow of gas into the burner chamber (Westerberg *et al.* 2011). Due to the complexity at the burner region the mesh is generated by tetrahedrons with a bulk spacing of approximately 90 mm and a near-wall spacing of approximately 30 mm. The near-wall region is 20 elements thick. An expansion ratio of 1.3 for each element is applied until the bulk spacing is reached. The inlet and the outlet region have the same grid size as the wall throughout the volume. The total number of nodes is $1.8 \cdot 10^6$ and the same mesh is used for the three different nozzle positions. The mesh for the present study was adjusted in order to reduce the number of elements with small angles and a high aspect ratio in order to facilitate the convergence of the solution. Figure 2 shows the mesh close to the burner region in the reactor where it is shown to have a well resolved mesh in order to capture the dynamics of the flow, particle transport and evaporation of droplets.

The calculations have been performed on the research groups own computer (parallel PC) cluster comprising 300 nodes and 12 single 8-node computers. Our ANSYS CFX licences cover full usage of the cluster.
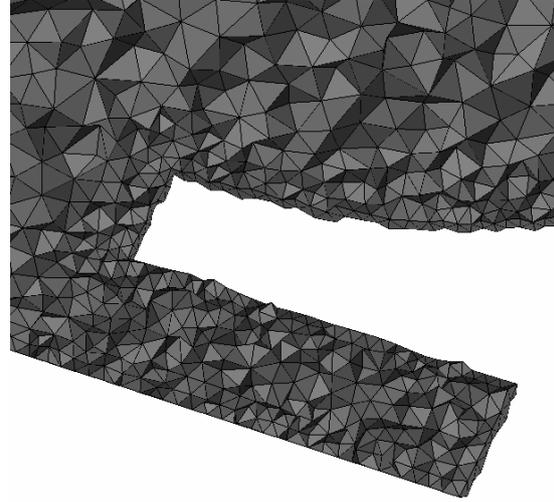
Fig. 2. The computational mesh near the burner region of the regeneration reactor.

4.3 Boundary conditions

The burner is simulated as an inlet of hot air at $1040°C$ where the gas is a mixture of air and $8.7\%_m$ (mass percentage) water vapour, which corresponds to the exhaust gas mixture. The mass flow is 0.77 kg/s. The outlet is modelled so that no gas can enter the domain and has a zero pressure difference, meaning the pressure is equal in the axial direction (see Fig. 1) immediately before and after the outlet opening considering a flow into the outlet which we want to avoid. With a higher pressure on the outside of the outlet entry, gas will enter the domain this way. The walls are modelled as smooth with a heat transfer coefficient of $0.6 \, W/K/m^2$. Each respective spray nozzle is modelled as a point source and the injected particles are considered normally distributed in size with a mean diameter of $370 \mu m$ and standard deviation of $100 \mu m$. A normal distribution is considered, since the exact size distribution is not known. Each particle consists of $49\%_m$ water and $51\%_m$ solids with densities of $958 \, kg/m^3$ and $1600 \, kg/m^3$, respectively. The solid density is set so that the density of the waste acid is $1240 \, kg/m^3$. The initial temperature of the particles is $60°C$. The boundary condition used for the particles as they collide with the reactor wall are that the particles will bounce back with the same angle as they hit the wall, and hence will not affect the mass and energy balance in the reactor as they collide with the wall.

Heat transfer through radiation is not considered. The reason for this is that radiation stands for less than $10\%_{\mathrm{m}}$ of the heat transfer. This result follows from the expression of the heat transfer due to radiation, given by

$$h_r = \frac{\sigma_b \varepsilon_m (T_1^4 - T_2^4)}{T_1 - T_2}, \tag{11}$$

where T_1 and T_2 are the particle temperature and surrounding region temperature respectively, σ_b the Stefan-Bolzmann constant, and ε_m the surface emissivity which can be approximated as unity. The corresponding contribution due to convection follows from the definition of the Nusselt number, which when solving for h_c results in

$$h_c = \frac{Nu \cdot k_f}{L}, \tag{12}$$

where k_f the thermal conductivity of the fluid, and L a characteristic length (here chosen as the reactor diameter). In ANSYS CFX the Ranz Marshall correlation (see Eq. 6) is used in the model for heat transfer. The R-M correlation shows that the Nusselt number for a droplet following the continuous phase streamlines is of the order of 2 since Re_p and the Pr are small. With a thermal conductivity of the continuous phase (considered having the thermal properties of air) of the order of 0.04 bar the h_r-h_c ratio is of the order of 0.1, meaning the heat transfer from radiation can be considered small and thus can be disregarded in the model.

4.4   Validity of Model Simplifications

In the present model, a mixture of air and vapour is used to represent the exhaust gas from the burners. The estimation of the mass fraction vapour is crucial since the specific heat of vapour significantly differs from air and a low fraction of vapour would imply that the droplets evaporate without boiling. The mixture of N_2, CO_2 and O_2 is of less importance since these gases have almost the same properties and can therefore be approximated as air with the properties of an ideal gas. To model the energy balances correctly, evaporation, heat loss through the walls and chemical reactions have to be modelled. The evaporation consumes the largest proportion of energy and is modelled in these simulations, as are the heat loss through the walls, which are estimated by deriving the heat transfer coefficient to $0.6\,\mathrm{W/m^2K}$.

The process chemistry is not considered in this study, neither is the full particle formation process. Instead, a simplified particle evaporation model has been used where the particle consists of water and a remaining solid fraction. A complete model of the formation of iron oxide from iron chloride is hence not present. The impact of these simplifications on the quality of the actual model is here further discussed. Considering a droplet from the injection into the reactor through the spray nozzles to the formed by-product, the droplet goes through a set of different stages: The evaporation process is generally divided between the evaporation of excess water and that of chemically bound water. The chemically bound water will split from the iron chloride molecule at higher temperature and with slower kinetics compared to the excess water, which leads to a changed evaporation process (Shiemann *et al.* 2012). This in turn may have an impact on the dynamics in the reactor. The particle motion can also be affected by the particle formation process, where typically the particles are formed as hollow spheres, leading to an increased cross section and a decreased density (Shiemann *et al.* 2012).

The present model without the process chemistry or the full particle formation process described above is considered as a first order solution of the flow dynamics as these two processes not alone dominate the flow dynamics in the reactor. The flow in the reactor is heavily steered by the swirl generated by the four gas burners placed symmetrically around the periphery of the reactor. The combustion of the injected droplets will affect the dynamics inside the reactor, mainly due to variations in the temperature which in turn will induce buoyancy effects, and ultimately affect the particle pathway, since the buoyancy effect mainly influences the vertical velocity. Nevertheless, the velocity in the azimuth direction is several orders of magnitude higher than the vertical velocity. Overall it is important to remember that the present study is a tool for understanding the dynamics inside the reactor in order to build an understanding of the regions inside the reactor that are important for the regeneration process and how the changed flow will affect the energy efficiency. Taking this scenario as a base for the results, we are convinced that the conclusions obtained with the model simplifications presented above are indeed valuable, not least for the engineering science community dealing with numerical modeling.

Another model simplification covers the reactor walls which are considered smooth, while the walls in the actual geometry are made of bricks and hence have a rough surface. A possible approach would be to include an artificial surface roughness, but as the roughness is not known and assumably not uniform in space and varies with time due to erosion, we have chosen to model the walls as smooth. Furthermore, it is likely that the roughness of the wall will affect the physics in the near-wall region (with a characteristic length scale of the order

of the roughness of the wall) in terms of vertical behaviour and particle agglomeration. The effect of the surface roughness on a more global scale in terms of the overall flow dynamics is however considered to be non-dominating, and as a consequence, the first order approach treated in this study comprises smooth walls.

5. RESULTS

In this section, results for the outlet temperature, temperature distribution and vertical velocity distribution in the regeneration reactor, together with the distribution of evaporated particles in the reactor, are presented for the three different positions of the spray nozzles. The four spray nozzles located at the top of the reactor are placed symmetrically along a circle centered on the center of the reactor. The nozzle positions considered in this study are: r = 0.5, 1.5 and 3 m, respectively.

5.1 Impact of Nozzle Position on Temperature Distribution and Droplet Evaporation

In terms of the energy efficiency of the drying process, the outlet temperature is a valid indicator. In Table 2, results are presented for the outlet temperature for three nozzle positions. It is shown that almost identical results are obtained for nozzle position $r = 0.5$ m and $r = 1.5$ m respectively, while a higher outlet temperature is derived when the spray nozzles are located at $r = 3$ m. An explanation for this result is that by placing the nozzles closer to the wall the particles will evaporate in a limited region close to the wall so that the temperature close to the wall will be lower due to droplet evaporation and cause cold air close to the wall to sink through the process, which in turn reduces the heat loss through the wall. For the scenario of a position close to the center, the core region in the upper part will be colder and cause cold air to sink in the inner region. These effects and an overview of the temperature and velocity distribution are seen in Figs. 3 and 4.
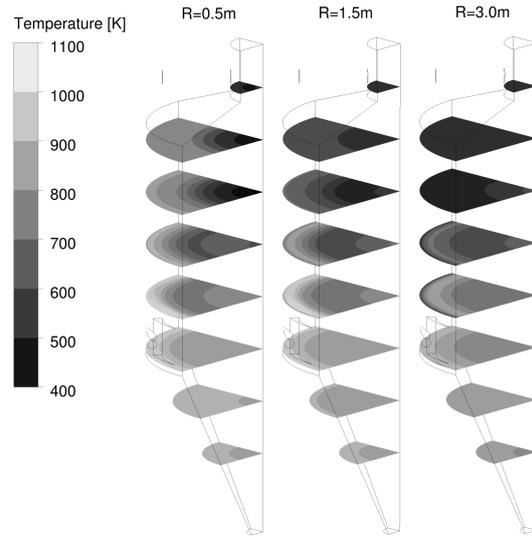
Fig. 3. Temperature distribution of the process for the different simulated cases with nozzle position at 0.5 m, 1.5 m and 3 m from center.
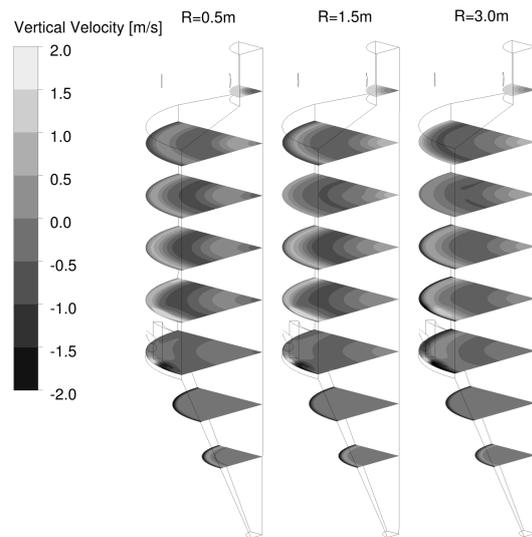
Fig. 4. Vertical velocity distribution in the process for the different nozzle positions, 0.5 m, 1.5 m and 3.0 m from the center.

Table 2 Results of the area averaged temperature for the different nozzle positions.

Outlet temperature			
Nozzle position	r=0.5 m	r=1.5 m	r=3.0 m
Temperature [K]	525.6	527.4	547.2

When the nozzles are placed close to the wall (r = 3 m), droplets will accumulate in the near-wall region before they are fully evaporated; see Fig. 5. This behaviour causes the temperature to be locally
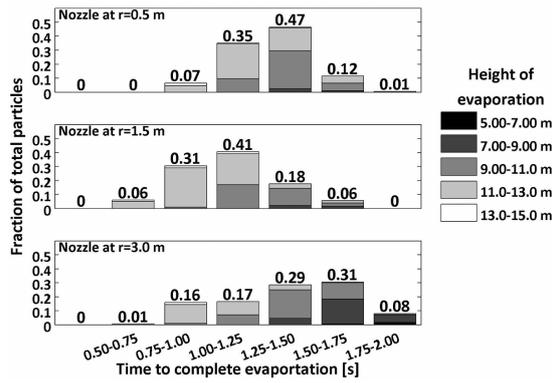
Fig. 5. Height position of fully evaporated particles. Each panel (diagram) represents different nozzle positions (from top to bottom): $r = 0.5$ m, $r = 1.5$ m and $r = 3.0$ m respectively. The y and x axes show the fraction of particles and time until fully evaporated and the grey scale indicates at which height the particles are evaporated.

Fig. 6. Radial position of fully evaporated particles. Each panel (diagram) represents different nozzle positions (from top to bottom): $r = 0.5$ m, $r = 1.5$ m and $r = 3.0$ m respectively. The y and x axes show the fraction of particles and time until fully evaporation, respectively, while the grey scale indicates at which radial position the particles are evaporated.

lowered, and consequently the time until full evaporation is extended; see Figs. 5 and 6. The sinking cold air close to the wall (Fig. 4) will transport the droplets down in the process so that the height when the particles are fully evaporated will be lower than the other nozzle positions (Fig. 5). By having the nozzle close to the center ($r = 0.5$ m) it will take longer for the particles to be transported and accumulated close to the wall. Since particles will be spread over a larger domain, the evaporation process will be faster, but with the result that hot gas from the burners will rise close to the wall. With nozzles placed 1.5 m from center, the droplets will be spread in a large volume and about 50% of them will evaporate close to the wall (Fig. 6), damping the rising of hot air close to the wall, and evaporation of those particles will be faster than with the other two nozzle positions. The height of evaporation is almost the same for nozzle position $r = 0.5$ m and $r = 1.5$ m but a slightly greater number of particles are transported further down in the process compared to the case with nozzle position $r = 0.5$ m.

5.2 Velocity and Temperature Variation of the Continuous Phase

From the results of the vertical velocity and temperature distribution presented in Figs. 3 and 4, it can be seen that these qualities are nearly constant in the azimuth direction. In order to better quantify the observed variation in the radial direction, the respective quantity is plotted along lines 1 and 2; see Figs. 1, 7, 8. In the near-wall region, 2 m below the nozzle, the vertical velocity is close to zero for nozzle position $r = 0.5$ m, while a negative velocity is observed for the other two positions. At the

level 1 m above the burner, negative velocities are only observed for nozzle position $r = 3$ m (Fig. 7). In the center region, the velocities are positive for nozzle position $r = 1.5$ m and $r = 3.0$ m, while the velocity is negative for nozzle position $r = 0.5$ m for both levels.

The impact of the nozzle position to the temperature distribution in the center region of the process is relatively small for both levels. However a small drop in temperature at the center with nozzle position $r = 0.5$ m is derived (Fig. 8). Close to the walls, the differences are larger where nozzle position $r = 3$ m shows a lower temperature. The results of the temperature and velocity distribution correlate well; a negative velocity in Fig. 7 indicates a low temperature, which is confirmed in Fig. 8.

6. DISCUSSION

The present study investigates the impact of the spray nozzle position on the energy efficiency of the regeneration process and the effect on the flow in the reactor with respect to the quality of the process by-product. The results in Figs. 5-8 show that the velocity and temperature distribution are strongly dependent on the nozzle position, and that a change in nozzle position will most likely optimize the process. The most energy-efficient position is to have the nozzles closer to the wall since this will cause particles to evaporate in a limited region in the vicinity of the wall so that the gas temperature in this region will be lower, and hence the gas will sink through the process, reducing heat loss through the wall. However, it is of importance that the particles do not stick and sinter at the wall, which can make flakes of Fe_2O_3 fall off the walls

and thereby destroy the process. This effect can be minimized by reducing the quantity of particles that evaporate close to the wall.
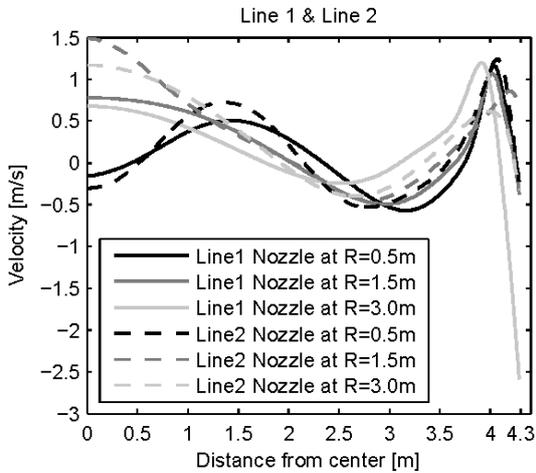
Fig. 7. Vertical velocities along two lines, Line 1 and Line 2, perpendicular to the wall, 8.8 m and 11.0 m from bottom.
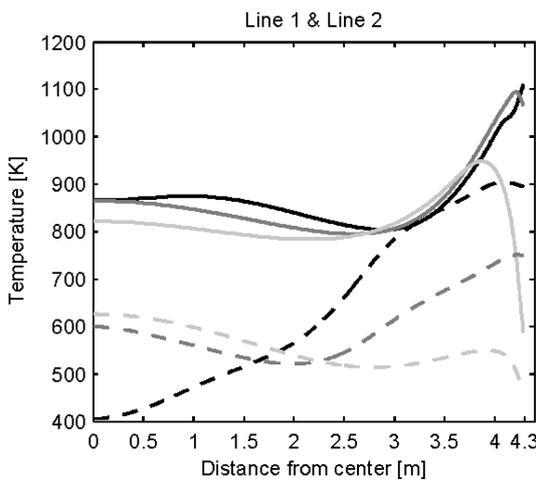
Fig. 8. Temperature along two lines, Line 1 and Line 2, perpendicular to the wall, 8.8 m and 11.0 m from bottom. Legends as in Fig. 7.

In order to produce good quality by-products it is assumed that all particles should go through the process with surroundings and exposure times that are as equal possible. This pre-condition means a narrow distribution in droplet evaporation position and time, and the droplets should evaporate before hitting the wall so that the risk of agglomeration at the wall is minimized. Running the process with nozzles at $r = 0.5$ m or $r = 1.5$ m indicates a production of a by-product of better quality. Comparing these two cases the results indicate that nozzle position $r = 1.5$ m gives a more dispersed particle evaporation time and positions compared to nozzle

position $r = 0.5$ m. Also, in order to avoid agglomeration at the wall for nozzle position $r = 0.5$ m, only a small fraction of the droplets are transported all the way to the wall before evaporation. Furthermore, in order to avoid particle agglomeration at the wall, a significant smaller fraction of the droplets are evaporated in the near wall region for nozzle position $r = 0.5$ m compared to $r = 1.5$ m.

Another measure which could have direct impact on the regeneration process efficiency is to keep the walls from being heated to too high a temperature. The wall temperature could be controlled by letting the spray cool down the wall, which would reduce heat loss through the wall and hence increase the process efficiency. In Table 2 it is shown that the case with a nozzle position at $r = 3$ m gives the best efficiency which in turn leads to reduced fuel consumption.

7. Concluding Remarks

In this work, the dynamics of a spray roasting process where Fe_2Cl_3 is regenerated to HCl has been modeled with a second order numerical scheme and a two-way coupled Eulerian- Lagrangian approach. The energy balances in the process are described with evaporation of droplets and heat loss through walls. Chemical reactions that appear in the process are not described. Results indicate that if a good quality by-product is of primary interest or to reduce particle agglomeration at wall, a nozzle position at a radial distance of 0.5 m from the reactor center line would be preferable. It is also shown that in order to increase the efficiency of the process, a prioritized nozzle position should be closer to the wall since this will lower the near-wall temperature and thus reduce heat loss.

The approach for future work is well outlined by the inclusion of the process chemistry and particle formation. Furthermore, future work is also to consider experimentally visualizing and measuring the in-flow. There are however several challenges connected to such an operation due to the very hostile environment inside the reactor.

References

Abrahamzon, B. and W. Sirigano (1988). Droplet vaporization model for spray combustion calculations. *International Journal of Heat and Mass Transfer 32*(9), 1605–

1608.

Avinash, K., J. A. Rao, Y. V. R. Kumar, and S. Sreenadh (2013). Bingham fluid flow through a tapered tube with permeable wall. *Journal of Applied Fluid Mechanics 6*(1), 131–141.

Beck, M., S. Wirtz, and V. Scherer (2007). Experimental and numerical studies of Fe_2O_3 particle formation processes in a flat flame burner. *Chemical Engineering and Technology 30*(6), 790–796.

Beck, M., S. Wirtz, V. Scherer, and F. Bärhold (2007). Numerical calculations of spray roasting reactor of the steel industry with special emphasis on Fe_2O_3 - particle formation. *Research Article A 30*(10), 1347–1354.

Choudhury, M. and G. Hazarika (2013). The effects of variable viscosity and thermal conductivity on mhd oscillatory free convective flow past a vertical plate in slip flow regime with variable suction and periodic plate temperature. *Journal of Applied Fluid Mechanics 4*(2, Special Issue), 1–8.

Ferziger, J. H. and M. Peric (2002). *Computational Methods for Fluid Dynamics*. Springer Verlag.

Gibson, C. and R. Schild (2009). Hydro- gravitational dynamics of planets and dark energy. *Journal of Applied Fluid Mechanics 2*(2), 35–41.

Huang, L., K. Kumar, and A. Mujumdar (2004). Simulations of a spray dryer fitted with a rotary disk atomizer using a three-dimensional computational fluid dynamic model. *Drying Technology 22*(6), 1489–1515.

Johansson, S. (2010). Cfd simulation of hydrochloric acid regeneration with a ruthner process. Master's thesis, Luleå University of Technology, Sweden.

Johansson, S., V. Geza, L. Westerberg, and A. Jakovics (2010, September). Characteristics of flow and temperature distribution in a ruthner process. In *Proceedings of the International Scientific Colloquium Modelling for Material Processing*, pp. 317–322.

Kladnig, W. (2008). New development of acid regeneration in steel pickling plants. *Journal of Iron and Steel Research International 15*(4), 1–6.

Launder, B. and D. Spalding (1974). The numerical computation of turbulent flows. *Computer Methods in Applied Mechanics and Engineering 3*, 269–289.

Lundström, T., J. Hellström, and E. Lindmark (2010). Flow design of guiding device for downstream fish migration. *River Research and Applications 26*(2), 166–182.

Marjavaara, B., T. Lundström, T. Goel, Y. Mack, and W. Shyy (2007). Hydraulic diffuser shape optimisation by multiple surrogate model approximations of pareto fronts. *Journal of Fluids Engineering 129*(9), 1228–1240.

Regel-Rosocka, M. (2010). A review on methods of regeneration of spent pickling solutions from steel processing. *Journal of Hazardous Materials 177*, 57–69.

Shiemann, M., S. Wirtz, V. Scherer, and F. Bärhold (2012). Spray roasting of iron chloride fecl2: laboratory scale experiments and a model for numerical simulation. *Powder Technology 228*, 301–308.

Shih, T., W. Liou, A. Shabbir, Z. Yang, and J. Zhu (1995). A new $k - \varepsilon$ eddy viscosity model for high reynolds number turbulent flows. *Computers & Fluids 24*, 227–238.

Sommerfeld, M., B. van Wachem, and R. Oliemans (2008). *ERCOFTAC Best Practice Guidelines for Computational Fluid Dynamics of Dispersed Multi- phase Flows*. ERCOFTAC.

Stouffs, P. (2011). Hot air engines. *Journal of Applied Fluid Mechanics Vol4*(2, Special Issue), 1–8.

Tosun, I. (2002). *Modelling in transport Phenomena*. Elsevier Science B.V.

Westerberg, L., V. Geza, A. Jakovics, and T. Lundström (2011). Burner backflow reduction in regeneration furnace. *Engineering Applications of Computational Fluid Mechanics 5*(3), 372–383.

Yakhot, V., S. Orszag, S. Thangam, T. Gatski, and C. Speziale (1992). Development of turbulence models for shear flows by a double expansion technique. *Physics of Fluids A 4*(7), 1510–1520.